ACS Photonics

Article

Cite This: ACS Photonics 2019, 6, 2223−2230

pubs.acs.org/journal/apchd5

Novel Terahertz Sources in the Form of Multispectral Resonators Boosted by Both Pump Light Local Field Enhancement and Terahertz Purcell Effect

Zhanghua Han,*,†,‡ Yangjian Cai,*,†,§ Uriel Levy,∥ and Sergey I. Bozhevolnyi⊥

†Shandong Provincial Engineering and Technical Center of Light Manipulations and Shandong Provincial Key Laboratory of Optics and Photonic Devices, School of Physics and Electronics, Shandong Normal University, Jinan 250358, China

‡Advanced Launching Co-innovation Center, Nanjing University of Science and Technology, Nanjing 210094, China

§School of Physical Science and Technology, Soochow University, Suzhou 215006, China

∥Department of Applied Physics, The Hebrew University of Jerusalem, Jerusalem, Israel

⊥Center of Nano-optics, University of Southern Denmark, Odense M, DK-5230, Denmark

ABSTRACT: Most terahertz sources nowadays are still inefficient and have low output powers, especially for the continuous-wave THz radiations in the 1−2 THz band, impeding the further development of terahertz science and its application in various fields. While considerable research effort has been made on the improvement of conversion efficiency from optical/electrical energy to terahertz radiations, less effort is made to maximize the extraction of terahertz energy from the chip to the far field. In this paper, we show a scheme that these two goals can be met simultaneously by making use of multispectral resonators, which resonate both in the terahertz band to improve terahertz extraction via Purcell effect and in the optical frequencies, exhibiting huge local field enhancement to improve the optical-to-terahertz conversion. Using the nonlinear process of difference frequency generation as an example, our results show that combing a large split-ring resonator (SRR) as a terahertz resonator and nanoscale bowtie optical antennas embedded in the SRR slit, an overall enhancement factor larger than 2×10^5 in the radiated terahertz power to the free space can be achieved compared to the case when the metallic structures are absent. This scheme of multispectral resonators can be extended to other terahertz sources, like the photoconductive antennas, and help realize more efficient terahertz sources.

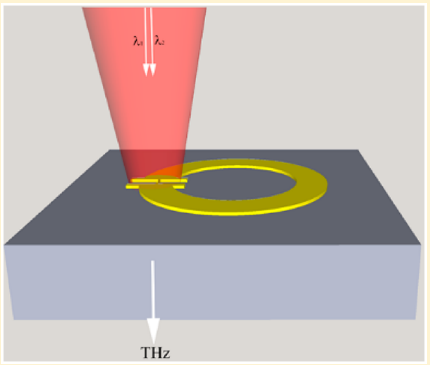

KEYWORDS: *terahertz generation, plasmonic slot waveguide, multispectral resonator, Purcell effect*

The past three decades has witnessed a great research effort in developing terahertz (THz) technology,[1] which is believed to hold the promise for a variety of applications, ranging from sensing[2] and communications[3] for applied sciences to the investigations of exciton behaviors[4] in solids for fundamental research. While researchers are still struggling nowadays to push forward the applications of THz technology in various fields like security checking, biomedical diagnosis, pharmaceutical analysis, gas sensing, and semiconductor chip failure analysis, the performances of these applications are still far from being acceptable. Hence, the original phenomenon of "THz gap", which describes the immature technological development in this spectral range, is still not fully eliminated. Although most THz components in a typical THz application system need further development, the most urgent issue is still how to further optimize the performance of portable THz emitters, especially for the continuous-wave (CW) form of THz radiations, which is indispensable for applications like THz communications and fast imaging. In particular, THz sources working in the CW form in the band of 1.0−2.0 THz are of special importance because of rich spectral information for the sensing application for many chemicals. To date many approaches have been explored to generate CW THz radiations, including both the electronics- and optics-based approaches. The former employs the use of multiple amplifiers and usually suffers from low spectral tunability and weak power beyond 1 THz (see, e.g., products from Virginia Diodes, Inc.), while the latter approach, including the second order nonlinear process of difference frequency generations (DFG),[5] photomixing based on ultrafast semiconductors[6] and ultrafast photodiodes,[7] also has various problems. For example, the regular DFG process needs to meet the phase-matching conditions, and the required nonlinear medium is usually bulky and hard to be incorporated into on-chip applications; photomixing devices and photodiodes have the same problem that the output THz power drops sharply as the frequency increases. It is still hard for the state-of-the-art quantum cascade lasers (QCL) to work below 2.0 THz, not to mention

Received: February 26, 2019
Published: August 27, 2019

DOI: 10.1021/acsphotonics.9b00322
ACS Photonics 2019, 6, 2223−2230

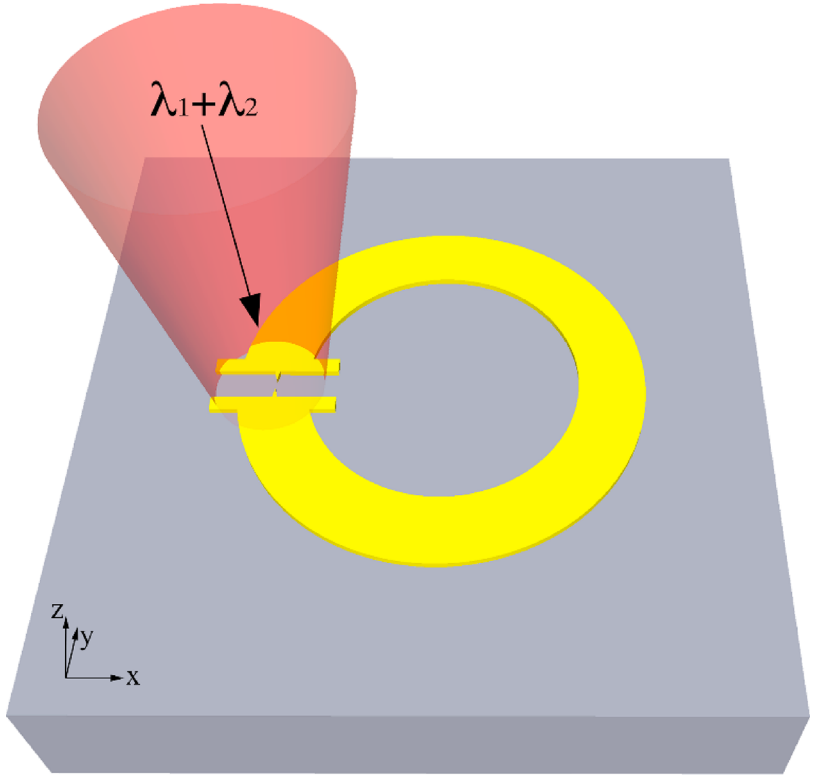

Figure 1. Schematic of the thin film THz sources incorporating both the SRR structure for THz Purcell effect and the plasmonic bowtie antenna to enhance the efficiency of the DFG process.

the cryogenic conditions that QCL requires, which is inconvenient for use.

Many approaches have been explored and reported to improve the CW THz source efficiency. For example, in the optics-based THz sources, plasmonic antennas resonating at the wavelength of the pump lights have been utilized to enhance the interactions between the lasers and the THz-generating medium.[8,9] As a result of the local electric field enhancement associated with the optical nanoantennas, an optical-to-THz conversion efficiency at 2 orders of magnitude higher has been experimentally demonstrated.[10] We need to note that two important issues must be considered when one aims at realizing an efficient THz source, to optimize the energy conversion from the electrical or optical signals to the THz, and to maximize the extraction of THz energy from the chip to the far field. While considerable research effort has been made on the former topic, less is done on the latter, especially for the THz output to free space. The application of optical nanoantennas as a transducer between free radiation and localized energy may give us a clue.[11] It is well-known that the spontaneous emission rates from a two-level system like excited fluorescence molecules or quantum dots can be significantly enhanced when the emitter is placed in close contact with a nanoantenna.[12] This enhancement can be well understood by the principle of reciprocity. A freely propagating light beam incident onto the nanoantenna will be concentrated to the near-field of the nanoantenna, exhibiting a huge local electric field enhancement.[11] If we assume the introduction of the antenna does not modify the radiation pattern of the emitter, then in contrast, the radiations from an emitter placed in the near field of the antenna will be propagating along the opposite routine back, with the power of several orders of magnitude higher to the far field than that from the same emitter placed in free space.[13] So the antenna provides more channels of energy transfer between the propagating waves and the localized radiations, and optical nanoantennas in various forms have been investigated for the purpose of optical spontaneous emission enhancement.[14] The main attribute of these antennas is the local electric field enhancement, which changes the local electromagnetic environment (photonic mode density) and the subsequent spontaneous emission rate according to Fermi's golden rule.[15] The same working principal can be extended to the THz band to improve the emission power by using another structure resonating at the THz frequencies, provided a similar local electric field enhancement can be achieved at THz frequencies. This enhancement is also known as the Purcell effect.

The large contrast between light and terahertz wavelengths lead to a mismatch in the dimension of structures required for enhancing light/matter interactions and for the THz Purcell effect, respectively. As a result, it is hard to meet both the two purposes using a single structure. In this work, we demonstrate the use of a multispectral resonator which have resonances both in the optical and THz frequencies. By combining the two effects of pump light local field enhancement and the terahertz Purcell effect associated with the two resonances, respectively, both the two processes of optical-to-THz conversion and THz coupling from chip to free space can be enhanced. Using a nonlinear process of DFG as an example, we numerically show an overall enhancement in final output power by a factor of 2×10^5 compared to the case when the pump lights imping on the bare nonlinear medium. The incorporation of two types of resonators with different scales into one structure represents a new routine of realizing efficient and ultracompact THz sources for practical applications.[16]

DOI: 10.1021/acsphotonics.9b00322
ACS Photonics 2019, 6, 2223−2230

STRUCTURE AND NUMERICAL APPROACH

The example structure for the DFG process is schematically shown in Figure 1, where two pump lights with slightly different wavelengths of λ_1 and λ_2 are focused onto the slot of a split ring resonator (SRR) structure. The SRR is made from gold and it resonates at the THz frequencies, while its narrow slot with the width of a few hundred nanometers can work as a plasmonic slot waveguide (PSW)[17,18] for the pump lights. The tight confinement of the PSW can help to enhance the nonlinear DFG process and the finite length of the slot (in the x direction) renders it a Fabry−Perot resonator. In particular, a number of optical nanoantennas can be incorporated into the slot, which also resonate at the two pump lights and help convert optical energy to the THz polarizations through the second order nonlinear process. It is worth noting that, for the two pump lights close to 1550 nm, a wavelength difference around 8 nm corresponds to the frequency of 1 THz. Due to the small quality factors of the plasmonic resonators in the telecom, both Fabry−Perot resonators and the bowtie antennas have a bandwidth of a few tens of nanometers. As a result, the enhancement from all the resonators works for both λ_1 and λ_2.

The simulation of the DFG process involves the mixing of electromagnetic fields at three different frequencies (f_1, f_2 corresponds to the two pump lights and $f_3 = f_1 - f_2$ is the THz frequency). In the simulations only the pump light fields are used as the inputs and the generated THz field E_3 is used to calculate the THz output power to the far field. The presence of the bowtie antennas and PSW strongly localizes the pump light fields to the bowtie area, while the SRR couples the generated THz field from the deep subwavelength volume to the far field in a reverse direction. As a result, the slow varying amplitude approximation which is widely adopted in nonlinear optics cannot be used. We model the whole process of DFG within the thin structure as a coupling between the two light fields $E_1(\vec{r})$, $E_2(\vec{r})$ and the THz field $E_3(\vec{r})$ using eqs 1−3, where $\varepsilon_1(\vec{r})$, $\varepsilon_2(\vec{r})$, and $\varepsilon_3(\vec{r})$ are the position-dependent permittivity at these three frequencies, k_1, k_2, and k_3 are the vacuum wave numbers, and $\chi^{(2)}$ is the second order nonlinear susceptibility of the nonlinear medium that is embedded within the slot. Note that on the right side of eqs 1−3, the term $e^{-j(k_1+k_2-k_3)z}$ is negelected considering the small thickness of the nonlinear medium. In practice, the efficiency of the DFG process is quite low, leading to a value of $E_3(\vec{r})$ much smaller than $E_1(\vec{r})$ and $E_2(\vec{r})$. As a result, the right-hand side of both eqs 1 and 2 can be neglected for simplification. The total problem can be reduced to the solving of two linear equations at f_1 and f_2, and the results of $E_1(\vec{r})$ and $E_2(\vec{r})$ can be used as the nonlinear source term in eq 3 to calculate the generate THz power.

$$\nabla \times (\nabla \times E_1(\vec{r})) - k_1^2 \varepsilon_1(\vec{r}) E_1(\vec{r}) = \omega_1^2 \varepsilon_0 \mu_0 \chi^{(2)} E_2(\vec{r}) \cdot E_3(\vec{r}) \quad (1)$$

$$\nabla \times (\nabla \times E_2(\vec{r})) - k_2^2 \varepsilon_2(\vec{r}) E_2(\vec{r}) = \omega_2^2 \varepsilon_0 \mu_0 \chi^{(2)} E_1(\vec{r}) \cdot E_3^*(\vec{r}) \quad (2)$$

$$\nabla \times (\nabla \times E_3(\vec{r})) - k_3^2 \varepsilon_3(\vec{r}) E_3(\vec{r}) = \omega_3^2 \varepsilon_0 \mu_0 \chi^{(2)} E_1(\vec{r}) \cdot E_2^*(\vec{r}) \quad (3)$$

The final THz radiations can be calculated using the commercial software of COMSOL Multiphysics. To reduce the requirement for computer memory, the light fields $E_1(\vec{r})$, $E_2(\vec{r})$ are restricted to a volume covering only the PSW and an additional length of 5 μm along the z direction to accommodate the light incidence, while the THz field $E_3(\vec{r})$ is calculated in the whole structure. A 10-layers of swept mesh is used to model the thin 200 nm metal layer. Within the XY plane, the mesh is set to make sure that the maximum mesh size is less than half the bowtie gap. With all these mesh settings, it is assured that the numerical results are convergent. From eq 3 one can see that the generated THz electric field is dependent on the local electric strength of E_1 and E_2, confirming the importance of using of optical antennas to enhance both E_1 and E_2 to get a maximum output of E_3.

The Purcell effect for the THz emission from the SRR structure works for the THz dipoles polarized along the y direction while the major electric field in both the PSW and the bowtie antenna is also along the same direction. As a result, a nonlinear medium with the $\chi_{ijk}^{(2)}(i = j = k)$ is required. We choose in this paper a nonlinear polymer and only consider its $\chi^{(2)} = 200$ pm/V along the y direction for simplicity. A polymer with an even higher $\chi^{(2)}$ is readily available[19] and has been experimentally utilized in a millimeter plasmonic mixer on the silicon platform.[20] To take into account the fact that the nonlinearity may deteriorate when the polymer is embedded in the metal slot, a value of 200 pm/V is used for the calculations. Although gold also has a second order surface susceptibility arising from the breaking of symmetry at surfaces, its susceptibility is much smaller. As a result, the much smaller contribution from the gold to the THz generation is not considered. We also note that, due to the large spectral difference between the pump lights and the THz radiations, there is a large distinction in the electromagnetic property for the same material in the two regimes. In our calculations, the tabulated experimental values from Johnson and Christy[21] is used for gold as the plasmonic material in the near-infrared while it is considered as a conductor (conductivity of 4.52×10^7 S/m) in the THz band. The nonlinear polymer is assumed to have an index of 1.673 for the pump lights, while its index is 1.5 at THz frequencies. The whole structure is on top of a quartz crystal substrate whose index is 2.0 in the THz band and 1.45 in the near-infrared, respectively.

In our calculations, we keep the wavelength of one pump light as a constant $\lambda_1 = 1550$ nm. To achieve a THz frequency of f_3, one just needs to adjust the wavelength λ_2 of the second pump. A plane wave is used for the two pump lasers in the simulation and the irradiance of both pump lights is assumed to be $I_0 = 0.0133$ GW/cm^2, which can still be practically implemented by focusing the CW pump lights onto a diffraction-limited spot. Note that the spot does not need to be smaller than the slit width, and it can be focused with a microscopy objective. In practice, the pump laser has a Gaussian beam profile and its width is diffraction-limited. Furthermore, the pump laser is usually set to cover the whole slit area. In that context, the subwavelength bowtie antenna has an area, which is much smaller than the beam size. Therefore, the plane wave is a good approximation in the numerical calculations. Only the power incident onto a single antenna will be used to calculate the optical-to-terahertz conversion efficiency. The electric field of this laser irradiance is still much smaller than the typical values from typical femtosecond lasers that will result in an ablation of the metal materials[22] and also smaller than the poling electric field that is required to achieve nonlinear property for polymers.[19] As a result, the laser density is safe for all the materials used in the simulations.

RESULTS

We first show the level of enhancement from Purcell effect associated with the SRR structure[23] for THz emission. It is

DOI: 10.1021/acsphotonics.9b00322
ACS Photonics 2019, 6, 2223−2230

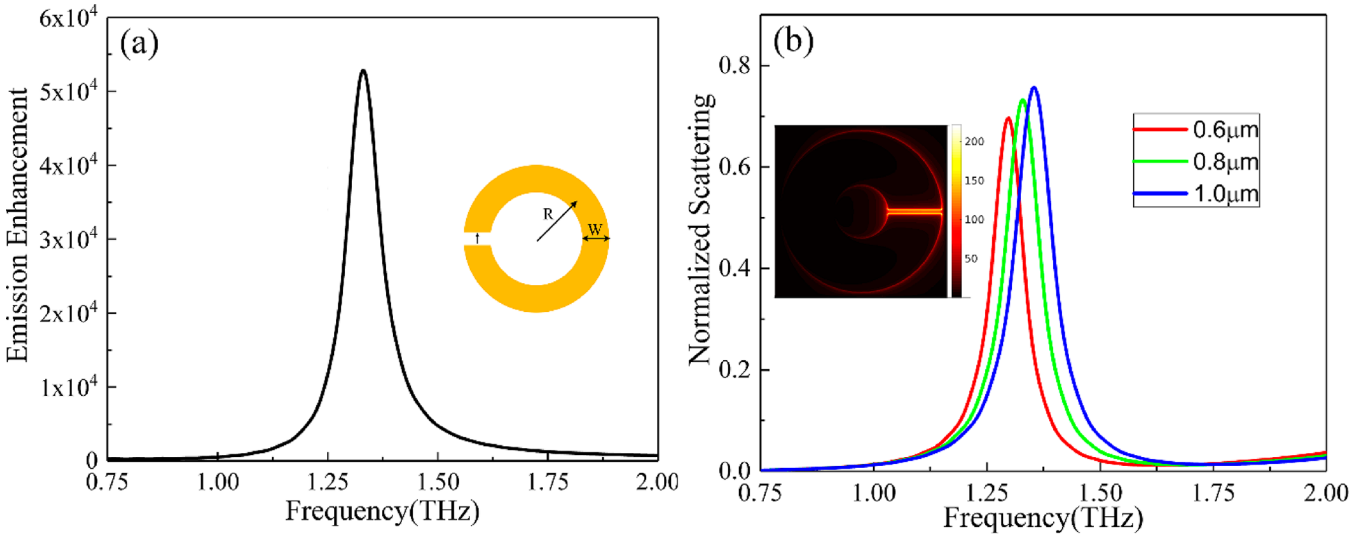

Figure 2. (a) Emission enhancement of THz radiation resulting from a SRR structure with 0.8 μm slit width. Inset: schematic of the SRR structure in which the small arrow indicates the point electric dipole. (b) Scattered power normalized to that from the incident THz radiations with different slot widths of 0.6, 0.8, and 1.0 μm. Inset: the electric field amplitude at the SRR resonance for the slot width of 0.8 μm. $R = W = 10$ μm for all the calculations.

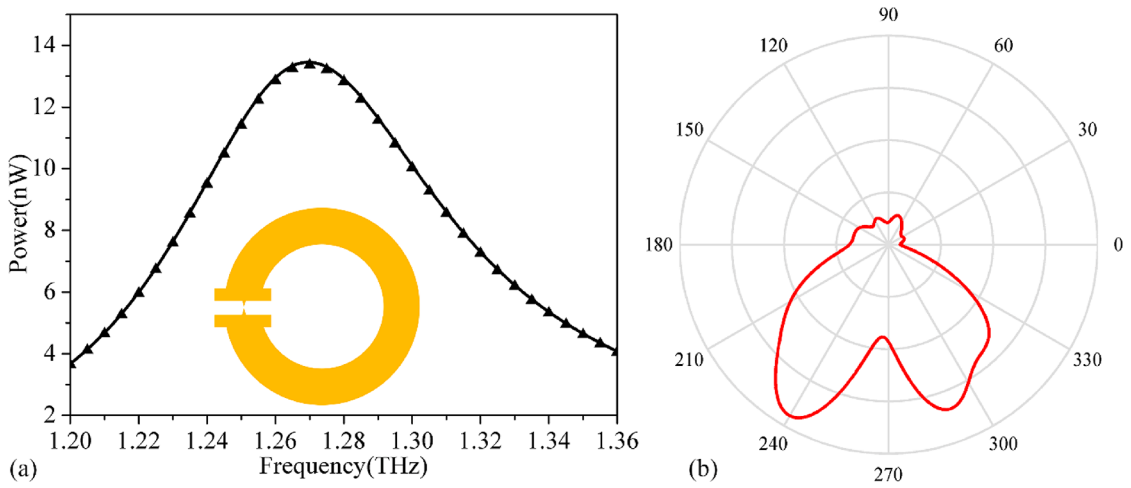

Figure 3. (a) Calculated THz output power when both the SRR and one bowtie antenna are present in the center of the slot. The solid line is from a fully coupled approach between two optical fields and the THz field, while the triangles represent results from the simplified approach. The inset is a schematic of the top view of the whole structure. The radius and strip width of the SRR are both 10 μm. (b) Radiation pattern of the THz electric field amplitude in the XZ plane containing the SRR slit.

known in the optical frequencies[24] that the power enhancement of the spontaneous emission (SE) from a two-level system can be calculated by using the radiative power P_{rad} from a point dipole to the far field when it is placed in the proximity of an antenna normalized to that from the dipole placed on the bare substrate, P^0_{rad}.

$$F = \frac{P_{rad}}{P^0_{rad}} \tag{4}$$

Following this procedure, we simulated the emission behavior using the finite-difference time-domain (FDTD) method. Note that other numerical methods like the FEM can also be used for the same calculation. FDTD is adopted here for its broadband and fast calculation capacity during a single simulation with the pulsed excitation. The SRR is made from 200 nm thick gold and the electric dipole is placed in the center of the 0.8 μm slit and on top of the quartz substrate. The polarization of the dipole is set perpendicular to the slit. One set of closed power monitors surrounding the whole structure are used to analyze P_{rad} from the dipole while the same monitors are used to calculate P^0_{rad} when the SRR is absent. Figure 2a presents the calculated emission enhancement for the SRR, which has a radius of $R = 10$ μm and width of $W = 10$ μm. It is quite clear that a significant enhancement more than 5×10^4 times by the SRR is observed in the emitted power from the dipole. To investigate the origin of the resonance for this emission enhancement, the scattering power from a single SRR structures normalized to the incident power from a plane wave polarized perpendicular to the slot edges is calculated as a function of frequency. The results for different slot widths of 0.6, 0.8, and 1.0 μm are shown in Figure 2b, exhibiting a significant shift of the resonance when the slot shrinks. These results suggest that inductance-capacitance (LC) resonance is responsible for the SRR resonance, with the capacitance strongly dependent on the slot width. The electric

DOI: 10.1021/acsphotonics.9b00322
ACS Photonics 2019, 6, 2223−2230

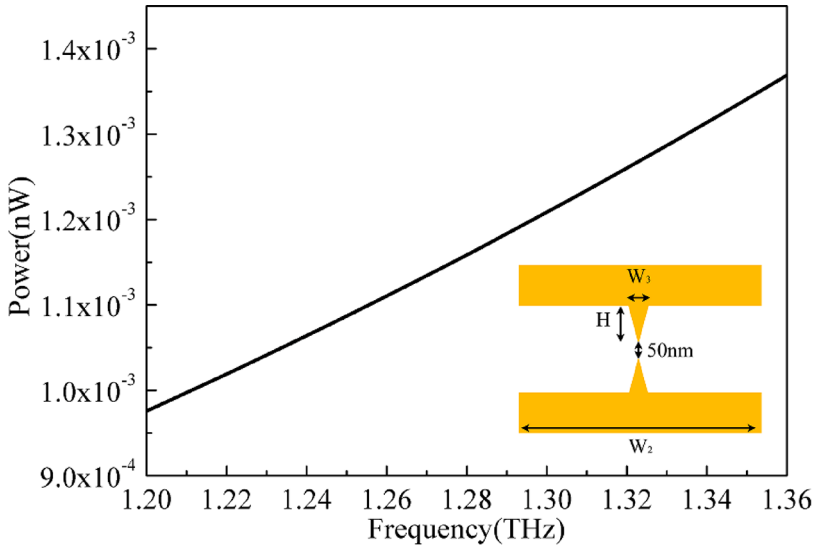

Figure 4. THz output power vs frequency when a single bowtie antenna is present in the center of the slot and the SRR is absent. The inset is a schematic of the top view of the whole structure.

field amplitude distribution is shown as the inset in Figure 2b for the slot width of 0.8 μm, where a local electric field enhancement more than 220 is observed within the slit. When the slot width is smaller, besides the fact that a higher electric field enhancement can be achieved in the slot, another interesting feature is that the scattering counterintuitively decreases while the area of the metallic part increases. This is because the LC resonance supported by the SRR with a circulating current loop can also be considered as a magnetic dipole resonance accompanied by the excitation of electric dipole, whose momentum is proportional to the slot width. Similar phenomenon has been discovered in the optical frequencies when a metal stripe supporting an electric dipole resonance is bent into a conformal geometry, which is in favor of magnetic-dipole resonance.[25]

The ideal THz dipole can be approximated using a bowtie antenna embedded into the slot, which is optimized to make sure that it can resonate and provide a large local electric field enhancement at both the wavelengths of λ_1 and λ_2. The bowtie antenna has a dimension at the order of 100 nm, which is deeply subwavelength compared to the emitted terahertz radiation (~240 μm in wavelength), rending it an effective terahertz dipole, and the results given in Figure 2 are instructive for the Purcell enhancement. In the details, the bowtie antenna is composed of two triangles and the tip-to-tip distance in the bowtie antenna is 50 nm to ensure a possible fabrication of the structure when the gold film thickness is 200 nm. A size of W_3 = 71 nm and H_3 = 289 nm is used (see the inset in Figure 4), while the dimension for the SRR is $R = W_1$ = 10 μm. Here the width of the SRR is increased to 12 μm (see the inset in Figure 3a) compared to that in Figure 2 for the purpose that more bowtie antennas can be accommodated within the slot.

The emitted terahertz power as a function of frequency from the SRR structure with one bowtie antenna at the center of the slot is presented in Figure 3a, where the solid line represents results from the fully coupled eqs 1−3, while the triangular-shaped dots are from eq 3 only. It is evident that the simplified approach can give the results with negligible discrepancy from the fully coupled approach, indicating that one can use the reduced approach for the calculations of THz output. From Figure 3a, it is seen that the overall THz output power is at the nW level, reaching a peak value of 13.5 nW at 1.27 THz. The resonance bandwidth is around 0.1 THz, the same as the value shown in Figure 2, indicating that the resonance in the output THz power is due to the bandwidth of the SRR structure. Here we define the conversion efficiency as follows:

$$\eta = \frac{\int \vec{S}_{\mathrm{THz}} \cdot \hat{n} da}{2 I_0 S} \tag{5}$$

where $\vec{S}_{\mathrm{THz}}$ is the poynting vector of the generated THz field, $\hat{n}$ is the unit vector normal to the surface of a set of power monitors enclosing the whole SRR structure. Note that S is the area of the bowtie antenna and I_0 is the incident field intensity for one pump light, leading to the reference optical power to be that incident onto the bowtie antenna exclusively. This is an extensively used approach when one calculates the efficiency of an optical nanoantenna,[26] which has a much smaller size than the excitation beam. Using eq 5 and the values in Figure 3a, one can calculate that the optical to THz conversion efficiency is 2.3 × 10^{-6}. For comparison, we replaced all the gold structures in the simulations by the same thickness of the nonlinear polymer, and in this case, the calculated THz output power is around 7 × 10^{-13} W, showing that the THz output boosted by both the pump light local field enhancement and the THz Purcell effect by a factor of 2 × 10^5. The radiation pattern of the THz electric field amplitude at 1.27 THz to the far field is plotted in Figure 3b. Our simulation results show that the main component of the THz electric field is still y-polarized, the same as the pump lasers even when the SRR and the bowtie antenna are present. The radiation pattern exhibits two main lobes along the critical angle between air and quartz, and the THz power can be collimated and focused by using a silicon hemisphere placed under the quartz substrate. Some asymmetry can be observed between the two main lobes, which can be expected because the slit only exists on the left half part of the SRR structure.

The THz frequency at which the output power reaches its maximum in Figure 3a can be easily tuned by using a SRR structure with a different radius. This does not affect the design of the bowtie antenna significantly when the frequency tuning

DOI: 10.1021/acsphotonics.9b00322
ACS Photonics 2019, 6, 2223−2230

is not large, because the bowtie antenna usually covers a bandwidth of several THz. To confirm the role of the SRR when the nonlinear polarization from DFG works as the THz origin instead of an ideal electric dipole, the SRR structure is removed and only the PSW with a single bowtie antenna remains the same. The calculated THz output power as a function of frequency is presented in Figure 4 and it is seen that overall power level decreases to pW, which is indeed 4 orders magnitude smaller than the results in Figure 3a. These results are consistent with the predictions in Figure 2, showing that the extraction of THz power from the local region to free space based on the Purcell effect is indeed very important to achieve THz sources with high output powers.

A direct incidence of the pump lights onto the SRR slot will result in a certain excitation of the PSW mode, which also contributes to the optical-to-terahertz generation. To distinguish the contribution from the PSW from that from the bowtie antenna, the antenna is removed and THz power from the 12 μm PSW is calculated for the same pump conditions. One can see from the results in Figure 5 that without the

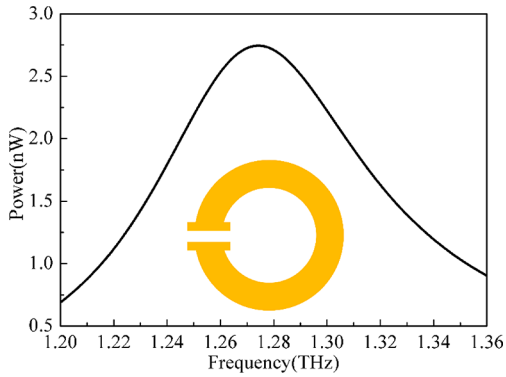

Figure 5. THz output power vs frequency when only the SRR is present while the bowtie antenna is absent. The inset is a schematic of the top view of the whole structure, whose radius and width are both 10 μm.

contribution from the bowtie antenna, the peak THz output power reaches only 2.75 nW at 1.27 THz. These results suggest that the single bowtie antenna can generate the THz power of 10.75 nW and is still 4× higher than that from the 12 μm long bare PSW. However, we note that the excitation efficiency of the PSW using a direct incidence of the pump lights onto the slot is quite low. When some coupling structures like gratings are introduced along the PSW, more coupling into the PSW and THz generation from the PSW with higher power can be expected.

The large stripe width of the SRR compared to the small footprint of a single bowtie antenna suggests that one can put more bowtie antennas into the same slot so that they can work simultaneously to generate even high THz power from the same pump lights.[9] When the antennas are arranged properly, they can emit THz in phase and in principle, a THz power $P = N^2P_0$ can then be expected, where P_0 is the THz power from a single antenna and N is the number of antennas. Although the bowtie antennas have a deep subwavelength volume compared to the THz radiations and can be considered as THz dipoles, we note that the slot in the SRR structure has a finite length, making it a Fabry–Perot resonator for λ_1 and λ_2. Standing wave patterns will be present due to the resonance, exhibiting an oscillation of both $E_1(\vec{r})$ and $E_2(\vec{r})$ with the periodicity between adjacent maxima indicated by $P = \lambda/(2n_{\text{eff}})$, where λ is the average between λ_1 and λ_2, and n_{eff}, the effective index of the plasmonic slot waveguide, is found to be 1.669 at 1550 nm. Then one can calculate the periodicity of the bowtie antenna to be around 460 nm. Although the introduction of the bowtie antennas may affect slightly the phase condition of the Fabry–Perot resonator, the calculated periodicity still represents an effective value for the antenna array. As an example, we use the number of bowtie antennas N = 3, with one located in the center of the slot while the other two resides on both sides with a distance P from the center. The periodicity P is shrunk to 450 nm because the presence of bowtie antennas with a narrower metal-to-metal gap will lead to a larger n_{eff} locally. In this case, the calculated THz power as a function of frequency is shown in Figure 6, where a peak power value of 75.5 nW is

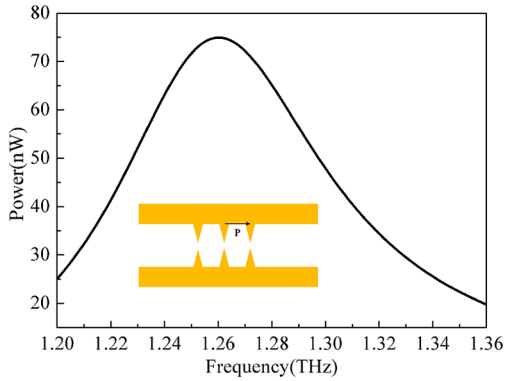

Figure 6. THz output power when there are three bowtie antennas located within the SRR slot. Inset: layout of the three bowtie antennas, note that the SRR is not shown for clarity.

achieved at the frequency of 1.26 THz. This power value is lower than N^2P_0 if we use the peak value in Figure 3 as the output from a single antenna, which we attribute to a nonuniform distributions of electric fields $E_1(\vec{r})$ and $E_2(\vec{r})$ along the slot. The slight red-shift of the peak frequency from 1.27 to 1.26 THz is a signature of the slight phase condition change within the SRR. These results indicate that a higher THz output power can indeed be expected when more bowtie antennas are introduced into the slot. For example, with the antenna periodicity of 460 nm and a slit length of 12 μm, an overall antenna number around 25 can be accommodated into the slit. If we use N^2P_0 for a rough estimation, a power as high as 8 μW can be achieved at around 1.26 THz, which is already superior to commercially available CW THz sources (cf. e.g., Terascan products working using 1550 nm excitation from Toptica Photonics).

DISCUSSIONS AND CONCLUSION

One can see from the above results that the Purcell effect can indeed enhance the output of THz power. Although the estimation of the Purcell factor based on the approach of using a point electric dipole in Figure 2 was originally proposed to characterize the change of the quantum emitter SE rate when it is placed in a different electromagnetic environment, and only QCL among popular THz sources can be classified into this category, we note that many THz sources based on the optical method can still be considered as general electric dipoles, like the change of photocurrent as a function of time in photoconductive antennas and photomixers and the nonlinear

DOI: 10.1021/acsphotonics.9b00322
ACS Photonics 2019, 6, 2223–2230

polarization density in optical rectification or DFG processes. So the same mechanism of combining the dual effects of the pump light local field enhancement and THz Purcell effect can be extended to different THz generation methods including the photoconductive antennas and photomixing, and other THz resonators, including dipole antenna and spoof surface plasmon based THz antennas.[27] The only drawback is that the emission enhancement only works at the THz antenna resonances, and a higher enhancement is usually associated with a narrower band. However, one can still use THz antennas that support multiple resonances;[28] then a broadband emission enhancement can still be realized. Furthermore, although we have demonstrated the enhancement of THz output power for CW form of THz radiations, we need to note that the same enhancement can also be used for pulsed THz generation, where a femtosecond laser with a higher peak electric field is used.

As a conclusion, we have shown in this paper that the multispectral resonators can indeed enhance the dual effects for both of the two processes, optical-to-terahertz conversion and the terahertz extraction from chip to space. Although multiresonant antennas have been used in the optical band for the generation of new frequencies,[29] to the best of our knowledge, this paper is one of the first demonstrations of a similar idea in THz generations. Using a bowtie antenna embedded into the slit of a SRR structure and the DFG process as an example, an overall enhancement in the final THz output by a factor of 2×10^5 has been numerically demonstrated compared to the case when the resonator is absent. This scheme of multispectral resonators can be extended to other THz sources like PCAs by properly designing the shape and dimension of the electrodes in the PCAs and help realize more efficient THz sources. Our results, together with other results reporting of manipulating THz radiation patterning and directionality by using a hyperbolic medium,[30] show that some ideas in optical nanoantennas and optical metamaterials can be efficiently extended to the THz band. Such concepts may become helpful in the quest for realization of on-chip THz sources with acceptable output power. We expect that these results will assist in paving the way for further development of THz technology, with the ultimate goal of bridging the THz gap.

AUTHOR INFORMATION

Corresponding Authors

*E-mail: zhan@sdnu.edu.cn.
*E-mail: caiyangjian@sdnu.edu.cn.

ORCID

Zhanghua Han: 0000-0002-4177-2555
Uriel Levy: 0000-0002-5918-1876
Sergey I. Bozhevolnyi: 0000-0002-0393-4859

Funding

This work is supported by the Natural Science Foundation of China (Project Nos. 51511140421, 11974221, 91750201, and 11525418).

Notes

The authors declare no competing financial interest.

REFERENCES

(1) Tonouchi, M. Cutting-Edge Terahertz Technology. *Nat. Photonics* **2007**, *1*, 97−105.
(2) Baxter, J. B.; Guglietta, G. W. Terahertz Spectroscopy. *Anal. Chem.* **2011**, *83*, 4342−4368.
(3) Ducournau, G.; Yoshimizu, Y.; Hisatake, S.; Pavanello, F.; Peytavit, E.; Zaknoune, M.; Nagatsuma, T.; Lampin, J. Coherent THz Communication at 200 GHz Using a Frequency Comb, UTC-PD and Electronic Detection. *Electron. Lett.* **2014**, *50*, 386−388.
(4) Scalari, G.; Maissen, C.; Turcinkova, D.; Hagenmuller, D.; De Liberato, S.; Ciuti, C.; Reichl, C.; Schuh, D.; Wegscheider, W.; Beck, M.; Faist, J. Ultrastrong Coupling of the Cyclotron Transition of a 2D Electron Gas to a THz Metamaterial. *Science* **2012**, *335* (6074), 1323−1326.
(5) Nishizawa, J.; Tanabe, T.; Suto, K.; Watanabe, Y.; Sasaki, T.; Oyama, Y. Continuous-Wave Frequency-Tunable Terahertz-Wave Generation From GaP. *IEEE Photonics Technol. Lett.* **2006**, *18*, 2008−2010.
(6) Preu, S.; Dohler, G. H.; Malzer, S.; Wang, L. J.; Gossard, A. C. Tunable, Continuous-Wave Terahertz Photomixer Sources and Applications. *J. Appl. Phys.* **2011**, *109*, 061301.
(7) Nagatsuma, T.; Ito, H.; Ishibashi, T. High-Power RF Photodiodes and Their Applications. *Laser Photonics Rev.* **2009**, *3*, 123−137.
(8) Berry, C. W.; Hashemi, M. R.; Preu, S.; Lu, H.; Gossard, A. C.; Jarrahi, M. Plasmonics Enhanced Photomixing for Generating Quasi-Continuous-Wave Frequency-Tunable Terahertz Radiation. *Opt. Lett.* **2014**, *39*, 4522.
(9) Lepeshov, S.; Gorodetsky, A.; Krasnok, A.; Rafailov, E.; Belov, P. Enhancement of Terahertz Photoconductive Antenna Operation by Optical Nanoantennas. *Laser Photonics Rev.* **2017**, *11*, 1600199.
(10) Tanoto, H.; Teng, J. H.; Wu, Q. Y.; Sun, M.; Chen, Z. N.; Maier, S. A.; Wang, B.; Chum, C. C.; Si, G. Y.; Danner, A. J.; Chua, S. J. Nano-Antenna in a Photoconductive Photomixer for Highly Efficient Continuous Wave Terahertz Emission. *Sci. Rep.* **2013**, *3*, 2824.
(11) Novotny, L.; van Hulst, N. Antennas for Light. *Nat. Photonics* **2011**, *5*, 83−90.
(12) Kinkhabwala, A.; Yu, Z.; Fan, S.; Avlasevich, Y.; Mullen, K.; Moerner, W. E. Large Single-Molecule Fluorescence Enhancements Produced by a Bowtie Nanoantenna. *Nat. Photonics* **2009**, *3*, 654−657.
(13) Rogobete, L.; Kaminski, F.; Agio, M.; Sandoghdar, V. Design of Plasmonic Nanoantennae for Enhancing Spontaneous Emission. *Opt. Lett.* **2007**, *32*, 1623−1625.
(14) Agio, M. Nanoscale Optical Antennas as Nanoscale Resonators. *Nanoscale* **2012**, *4*, 692−706.
(15) Barnes, W.L.; Bjork, G.; Gerard, J.M.; Jonsson, P.; Wasey, J.A.E.; Worthing, P.T.; Zwiller, V. Solid-State Single Photon Sources : Light Collection Strategies. *Eur. Phys. J. D* **2002**, *18*, 197−210.
(16) Chettiar, U. K.; Engheta, N. Optical Frequency Mixing through Nanoantenna Enhanced Difference Frequency Generation- Metatronic Mixer. *Phys. Rev. B: Condens. Matter Mater. Phys.* **2012**, *86*, 075405.
(17) Liu, L.; Han, Z.; He, S. Novel Surface Plasmon Waveguide for High. *Opt. Express* **2005**, *13*, 1976−1980.
(18) Han, Z.; Elezzabi, A. Y.; Van, V. Experimental Realization of Subwavelength Plasmonic Slot Waveguides on a Silicon Platform. *Opt. Lett.* **2010**, *35*, 502−504.
(19) Enami, Y.; Derose, C. T.; Mathine, D.; Loychik, C.; Greenlee, C.; Norwood, R. A.; Kim, T. D.; Luo, J.; Tian, Y.; Jen, A. K.-Y.; Peyghambarian, N. Hybrid Polymer/Sol − Gel Waveguide Modulators with Exceptionally Large Electro-Optic Coefficients. *Nat. Photonics* **2007**, *1*, 180−185.
(20) Salamin, Y.; Baeuerle, B.; Heni, W.; Abrecht, F. C.; Josten, A.; Fedoryshyn, Y.; Haffner, C.; Bonjour, R.; Watanabe, T.; Burla, M.; et al. Microwave Plasmonic Mixer in a Transparent Fibre-Wireless Link. *Nat. Photonics* **2018**, *12*, 749−753.
(21) Johnson, P. B.; Christy, R. W. Optical Constants of the Noble Metals. *Phys. Rev. B* **1972**, *6*, 4370.

DOI: 10.1021/acsphotonics.9b00322
ACS Photonics 2019, 6, 2223−2230

(22) Polyushkin, D. K.; Hendry, E.; Stone, E. K.; Barnes, W. L. THz Generation from Plasmonic Nanoparticle Arrays. *Nano Lett.* **2011**, *11*, 4718−4724.
(23) Tanaka, K.; Plum, E.; Ou, J. Y.; Uchino, T.; Zheludev, N. I. Multifold Enhancement of Quantum Dot Luminescence in Plasmonic Metamaterials. *Phys. Rev. Lett.* **2010**, *105*, 351−354.
(24) Novotny, L.; Hecht, B. *Principles of Nano-Optics*; Cambridge University Press, 2006.
(25) Della Valle, G.; Søndergaard, T.; Bozhevolnyi, S. I. Efficient Suppression of Radiation Damping in Resonant Retardation-Based Plasmonic Structures. *Phys. Rev. B: Condens. Matter Mater. Phys.* **2009**, *79*, 113410.
(26) Carletti, L.; Locatelli, A.; Stepanenko, O.; Leo, G.; De Angelis, C. Enhanced Second-Harmonic Generation from Magnetic Resonance in AlGaAs Nanoantennas. *Opt. Express* **2015**, *23*, 26544−26550.
(27) Han, Z.; Zhang, Y.; Bozhevolnyi, S. I. Spoof Surface Plasmon-Based Stripe Antennas with Extreme Field Enhancement in the Terahertz Regime. *Opt. Lett.* **2015**, *40*, 2533.
(28) Pors, A.; Moreno, E.; Martin-Moreno, L.; Pendry, J. B.; Garcia-Vidal, F. J. Localized Spoof Plasmons Arise While Texturing Closed Surfaces. *Phys. Rev. Lett.* **2012**, *108*, 223905.
(29) Aouani, H.; Navarro-Cia, M.; Rahmani, M.; Sidiropoulos, T. P. H; Hong, M.; Oulton, R.; Maier, S. Multiresonant Broadband Optical Antennas As Efficient Tunable Nanosources of Second Harmonic Light. *Nano Lett.* **2012**, *12*, 4997−5002.
(30) Feng, X.; Gong, S.; Zhong, R.; Zhao, T.; Hu, M.; Zhang, C.; Liu, S. Terahertz Radiation in Graphene Hyperbolic Medium Excited by an Electric Dipole. *Opt. Lett.* **2018**, *43*, 1187−1190.

DOI: 10.1021/acsphotonics.9b00322
ACS Photonics 2019, 6, 2223−2230